Metrologia

Absolute frequency measurement of the $^{1}S_{0}$–$^{3}P_{0}$ transition of ^{171}Yb with a link to international atomic time

OPEN ACCESS
IOP Publishing
Metrologia

Metrologia **57** (2020) 035007 (11pp)
https://doi.org/10.1088/1681-7575/ab50e8

Absolute frequency measurement of the $^1S_0$–$^3P_0$ transition of ^{171}Yb with a link to international atomic time

Marco Pizzocaro[1], Filippo Bregolin[1], Piero Barbieri[1,2], Benjamin Rauf[1,3], Filippo Levi[1] and Davide Calonico[1]

[1] Istituto Nazionale di Ricerca Metrologica (INRIM), Strada delle Cacce 91, 10135 Torino, Italy
[2] Politecnico di Torino, Corso duca degli Abruzzi 24, 10129 Torino, Italy

E-mail: m.pizzocaro@inrim.it

Received 1 August 2019, revised 8 October 2019
Accepted for publication 24 October 2019
Published 14 May 2020

Abstract

We report the absolute frequency measurement of the unperturbed optical clock transition $^1S_0$–$^3P_0$ in ^{171}Yb performed with an optical lattice frequency standard. Traceability to the International System of Units is provided by a link to International Atomic Time. The measurement result is 518 295 836 590 863.61(13) Hz with a relative standard uncertainty of 2.6×10^{-16}, obtained operating our ^{171}Yb optical frequency standard intermittently for 5 months. The ^{171}Yb optical frequency standard contributes with a systematic uncertainty of 2.8×10^{-17}.

Keywords: optical frequency standards, international atomic time, frequency metrology

(Some figures may appear in colour only in the online journal)

1. Introduction

Cesium fountains are the best realization of the second in the International System of Units (SI) [1]. Frequency standards based on optical transitions of several ions and atoms can outperform Cs standards in accuracy and stability [2–4] and a redefinition of the SI second based on an optical transition is anticipated [5]. In preparation, eight optical transitions are recommended as secondary representation of the SI second [6], with uncertainties comparable to those of Cs standards. Their values are calculated by a least square fit of absolute frequency measurements and frequency ratios involving optical frequency standards [7]. New ratio and frequency measurements are fundamental to improve the uncertainty of secondary representations of the second and to check the consistency of optical frequency standards.

Absolute frequency measurements are usually performed relative to Cs fountains that provide the local realization of the SI second. When a local Cs fountain is unavailable, absolute frequency measurements of optical standards are possible via international atomic time (TAI) [8–19]. TAI is a timescale maintained by the International Bureau of Weights and Measures (BIPM) from the satellite-based comparison of frequency standards in about 85 world-wide laboratories [20]. The BIPM computes TAI in 5-day intervals and publishes monthly its frequency deviation from the SI second in the Circular T bulletin [21]. The BIPM also disseminates coordinated universal time (UTC), the international timescale recommended for civil use, which differs from TAI only by an integer number of leap seconds [20].

Conversely, optical frequency standards can contribute to TAI as secondary representations of the second, although few optical frequency standards have contributed so far: the ^{87}Sr frequency standards at the Laboratoire national de métrologie et d'essais–Système de Références Temps–Espace (LNE-SYRTE) [22], the ^{87}Sr frequency standard at the National Institute of Information and Communications Technology (NICT) [23] and the ^{171}Yb frequency standards at the National Institute of Standards and Technology (NIST) [2].

[3] Present address: Universität Bonn, Physikalisches Institut, Wegelerstrasse 8, 53115 Bonn, Germany

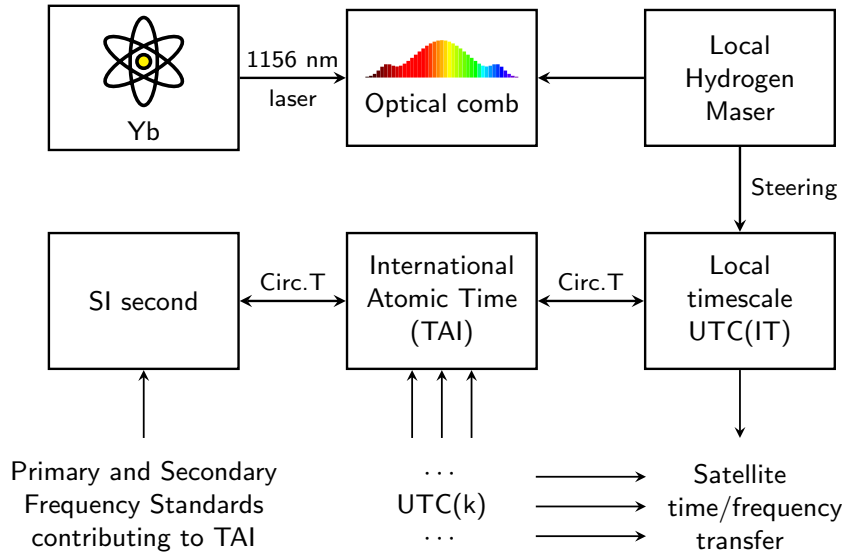

Figure 1. Overview of the frequency chain between the ^{171}Yb optical frequency standard to the SI second.

Among the optical secondary representations of the second is the frequency of the forbidden $^1S_0$–$^3P_0$ transition in ^{171}Yb. Here we present a measurement of this frequency obtained operating a ^{171}Yb optical frequency standard for 5 months where traceability to the SI is provided by a link to TAI. During this period, the ^{171}Yb optical frequency standard was operated only intermittently for a few hours at a time. Without a continuous measurement of the optical frequency [24], we used flywheels based on a hydrogen maser and TAI to account for the correction and uncertainty introduced by dead times in the operation of the optical frequency standard [11, 25, 26]. We also present an updated evaluation of the systematic uncertainty of the ^{171}Yb optical frequency standard, that was previously characterized for a measurement relative to the local Cs fountain ITCsF2 [27, 28] and for an optical frequency ratio with a transportable ^{87}Sr frequency standards developed by the Physikalisch–Technische Bundesanstalt (PTB) [29].

This paper is organized as follows. Section 2 presents an overview of the Yb optical lattice frequency standard and of the frequency chain to the SI. The evaluation of the systematic frequency shifts of the ^{171}Yb frequency standard is presented in section 3. Section 4 presents the evaluation of the uncertainty in the link to TAI and the data analysis, including the contribution from dead times. We report and discuss the results in section 5.

2. Experiment overview

Our ^{171}Yb optical lattice frequency standard has been described previously in [27]. A beam of Yb atoms is produced in an ultra-high-vacuum chamber from an atomic oven. Atoms from the beam are trapped and cooled in a two-stage magneto-optical trap, first using the $^1S_0$–$^1P_1$ transition at 399 nm and then using the weaker $^1S_0$–$^3P_1$ transition at 556 nm. A slower beam at 399 nm counter-propagating the atomic beam is used to increase the number of trapped atoms. Atoms are then loaded in a horizontal, one-dimensional optical lattice at the magic wavelength of 759 nm with a beam waist radius of 45 µm and a depth between 220 E_r and 400 E_r (where $E_r \approx h \times 2$ kHz is the recoil energy of a lattice photon and h is the Planck constant). Approximately 1000 atoms are trapped in about 1200 lattice sites with a temperature of 10 µK. Atoms are prepared in either single-spin ground state ($m_F = \pm 1/2$) with 98% efficiency by optical pumping on the $^1S_0$–$^3P_1$ transition. The clock laser at 578 nm is obtained by second-harmonic generation of a diode laser at 1156 nm. It is stabilized on a horizontal ultrastable cavity made in ultra-low-expansion glass with a length of 10 cm [30]. This setup has been improved compared to our previous work that used a different cavity [27]. The lattice polarization and the clock-laser polarization are aligned with the vertical magnetic field. We perform Rabi spectroscopy on the $^1S_0$–$^3P_0$ clock transition at 578 nm using a π-pulse of resonant light lasting 80 ms that results in a Fourier-limited linewidth of 10 Hz. The transition probability is measured by detecting the fluorescence from pulses of 399 nm light with a photomultiplier tube. In the detection we use a laser at 1389 nm to pump the atoms from the excited to the ground state, through the $^3D_1$–$^3P_1$ channel, renormalizing the number of excited atoms to the total number of trapped ones. A single operation cycle usually lasts 300 ms. The frequency of the 578 nm laser is tuned on resonance with the two π-transitions $^1S_0(m_F = \pm 1/2)$–$^3P_0(m_F = \pm 1/2)$ by acting on an acousto-optic modulator.

We achieved traceability of the ^{171}Yb frequency to the SI through the chain shown in figure 1. The 1156 nm cavity-stabilized laser is sent to a fibre frequency comb [31] by a noise-compensated fibre link [32]. The comb has a repetition rate of 250 MHz and is referenced to the 10 MHz output of a hydrogen maser. Fibre links and acousto-optic modulators are referenced to the hydrogen maser as well. The beatnote between the laser and the comb is redundantly measured to detect and remove cycle slips. The frequency ratio between the ^{171}Yb transition and the hydrogen maser frequency is calculated from the comb measurement, accounting for the

acousto-optic modulator used for steering and the second-harmonic generation stage.

The same maser is steered every 1 h to generate the local timescale UTC(IT) using an auxiliary output generator. Occasionally the steering is subject to frequency steps or changes in the drift rate to maintain agreement with UTC.

The local timescale UTC(IT) is compared continuously by satellite time and frequency transfer [33] to the timescales generated in other laboratories (denoted in figure 1 as UTC(k)). The BIPM calculates the time difference between UTC(IT) and UTC every 5 days from satellite transfer data and publishes them monthly in the Circular T [34]. The frequency difference between UTC(IT) and TAI can be calculated from the Circular T data (with the frequency of UTC equal to the frequency of TAI [20]).

TAI is a realization of terrestrial time (TT), a coordinate time scale defined in a geocentric reference frame with scale unit the SI second on a specific equipotential surface [35]. The BIPM calculates the fractional deviation of the scale interval of TAI from that of TT using the contributions of primary and secondary frequency standard participating in TAI. This deviation is calculated over one-month intervals, is published in the Circular T and provides the last step from TAI to the SI unit of frequency.

In summary, the measurement model is

$$\frac{f(\mathrm{Yb})}{f(\mathrm{SI})} = \frac{f(\mathrm{Yb})}{f(\mathrm{HM})}\frac{f(\mathrm{HM})}{f(\mathrm{UTC(IT)})}\frac{f(\mathrm{UTC(IT)})}{f(\mathrm{TAI})}\frac{f(\mathrm{TAI})}{f(\mathrm{SI})}, \quad (1)$$

where $f(\mathrm{Yb})$, $f(\mathrm{HM})$, $f(\mathrm{UTC(IT)})$, $f(\mathrm{TAI})$ are the frequency of the ^{171}Yb clock transition, of the local hydrogen maser, of UTC(IT) and TAI respectively and where we have formally wrote the SI unit of frequency as $f(\mathrm{SI}) = 1$ Hz. We calculated the frequency ratio between the ^{171}Yb transition and the hydrogen maser from the comb measurement. The frequency ratio between the hydrogen maser and UTC(IT) is calculated from the steering of the timescale. The frequency ratios between UTC(IT) and TAI and between TAI and the SI are calculated from data in the Circular T.

However, the frequency ratios appearing on the right hand side of equation (1) cannot be calculated for the same averaging time because of the intermittent operation of the optical frequency standard. The measurement model is expanded to consider extrapolation of the frequency ratios as:

$$\begin{aligned}\frac{f(\mathrm{Yb})}{f(\mathrm{SI})} = {} & \frac{f(\mathrm{Yb},\mathcal{T}_1)}{f(\mathrm{HM},\mathcal{T}_1)} \times \frac{f(\mathrm{HM},\mathcal{T}_1)}{f(\mathrm{HM},\mathcal{T}_2)} \times \frac{f(\mathrm{HM},\mathcal{T}_2)}{f(\mathrm{UTC(IT)},\mathcal{T}_2)} \\ & \times \frac{f(\mathrm{UTC(IT)},\mathcal{T}_2)}{f(\mathrm{TAI},\mathcal{T}_2)} \times \frac{f(\mathrm{TAI},\mathcal{T}_2)}{f(\mathrm{TAI},\mathcal{T}_3)} \times \frac{f(\mathrm{TAI},\mathcal{T}_3)}{f(\mathrm{SI},\mathcal{T}_3)},\end{aligned} \quad (2)$$

where $\mathcal{T}_1$, $\mathcal{T}_2$, $\mathcal{T}_3$ are the time periods, possibly discontinuous, in which each measurement is performed. Here $\mathcal{T}_1$ corresponds to the period of operation of the ^{171}Yb frequency standard while $\mathcal{T}_2$ and $\mathcal{T}_3$ have to be aligned with the 5-day grid and 1-month grid of Circular T respectively. The ratios $f(\mathrm{HM},\mathcal{T}_1)/f(\mathrm{HM},\mathcal{T}_2)$ and $f(\mathrm{TAI},\mathcal{T}_2)/f(\mathrm{TAI},\mathcal{T}_3)$ accounts for the extrapolations at different time periods exploiting the hydrogen maser and TAI as flywheels. The equality in equation (2) holds formally true because we assume the ^{171}Yb frequency and the SI unit of frequency constant in time.

Table 1. Uncertainty budget for ^{171}Yb optical frequency standard.

Effect	Rel. Shift$\times 10^{17}$	Rel. Unc.$\times 10^{17}$
Density shift	−5.9	0.2
Lattice shift	7.6	2.0
Zeeman shift	−0.693	0.014
Blackbody radiation	−235.0	1.2
Blackbody radiation oven	−1.7	0.8
Static Stark shift	−1.6	0.9
Background gas shift	−0.5	0.2
Probe light shift	0.09	0.05
Servo error	—	0.3
Fibre links	—	0.01
Line pulling	—	0.02
Tunnelling	—	0.4
AOM switching	—	0.4
Gravitational redshift	2599.5	0.3
Total	2361.8	2.8

3. Frequency shifts and uncertainties of the ^{171}Yb frequency standard

The analysis of the systematic frequency shifts in the ^{171}Yb frequency standard is summarized in table 1. We separately calculated the shifts for each run of the ^{171}Yb frequency standard. Table 1 reports the average over the whole measurement campaign.

3.1. Density shift

The density shift is evaluated by interleaving measurements with different number of atoms by changing the duration of the slower beam pulse at 399 nm during the first stage magneto-optical trap. This method does not impact the trapping conditions and we assumed the density shift to be proportional to the number of atoms [36]. However, the density shift depends on lattice depth [37], mean excitation fraction [38], degree of spin-polarization [2], pulse-area of the Rabi spectroscopy [39] and compression of the last magneto-optical trap stage before loading atoms in the lattice [40]. To account for all these effects, interleaved density measurements were repeated daily to characterize the specific trapping condition. During the campaign the atomic density ranged from $0.25\rho_0$ to $7\rho_0$, where $\rho_0 \approx 4 \times 10^{14}$ m^{-3} corresponds to about one atom per lattice site. We have not observed significant changes in the density shift during single runs and the typical instability of these measurements is $2.7 \times 10^{-15}(\tau/\mathrm{s})^{-1/2}$ as shown in figure 2. We can constrain the density shift uncertainty at low density to typically $<2 \times 10^{-17}$ for each day. As each daily density shift determination is independent, we consider this noise statistical and the shift averages to $-5.9(2) \times 10^{-17}$ for the campaign. We note that the density shift can be reduced

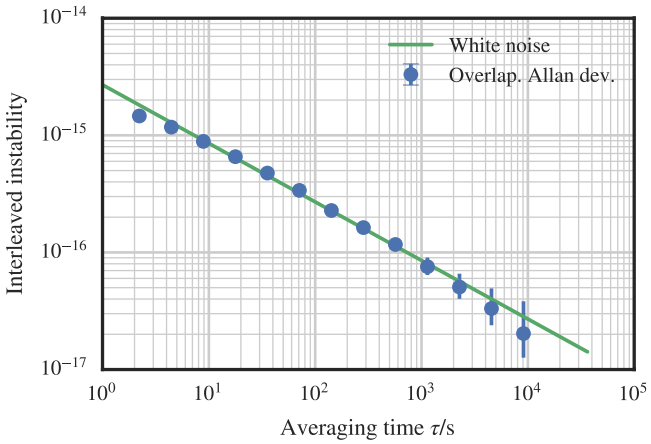

Figure 2. Example of the instability of an interleaved measurement used to evaluate the density shift. Blue dots are the overlapping Allan deviation of the relative frequency difference between high and low density during a single run of 53 000 s. The green line corresponds to white frequency noise as $2.7 \times 10^{-15}(\tau/\mathrm{s})^{-1/2}$.

at the $\times 10^{-18}$ level by working with lower trap depths, larger lattice waists or lower atom numbers [2, 41].

3.2. Lattice light shifts

The lattice shift is calculated from the model [41, 42]:

$$\Delta\nu_{\mathrm{ls}} = -\left(a\Delta\nu + \frac{3}{4}d(2n^2+2n+1)\right)\frac{U_\mathrm{e}}{E_\mathrm{r}} - d\left(\frac{U_\mathrm{e}}{E_\mathrm{r}}\right)^2 + (a\Delta\nu - b)\left(n+\frac{1}{2}\right)\left(\frac{U_\mathrm{e}}{E_\mathrm{r}}\right)^{1/2} + d(2n+1)\left(\frac{U_\mathrm{e}}{E_\mathrm{r}}\right)^{3/2}, \quad (3)$$

where $\Delta\nu$ is the lattice frequency detuning from the magic frequency, $U_\mathrm{e} = \xi U_0$ is the effective longitudinal trap depth that takes into account the reduced laser intensity seen by the atoms due to radial motion instead of the maximum trap depth U_0. The coefficient a is the slope between the differential polarizability and the lattice frequency, while b is the combined multipolar polarizability, and d the hyperpolarizability coefficient. The average longitudinal motional state in the lattice is indicated by n.

In the model we constrained $b = 0.08(8)$ mHz [43] and the hyperpolarizability $d = -1.04(9)$ µHz. We measured the value d from the light shift at lattice frequency near two-photon transitions, following the method described in [44, 45]. Away from the magic wavelength the clock line is broadened and asymmetric [46] and, for each two-photon transition, we fitted the barycenter of the line as a function of lattice frequency with a dispersion curve. The fit is used to extrapolate the shift to the magic wavelength. Equation (3) is then used to convert the shift to the coefficient d, from the measured trapping conditions U_0, ξ and n, including their uncertainties. The transitions observed, including hyperfine components, and their contributions to hyperpolarizability are summarized in table 2. This measurement is in agreement with other two-photon measurements [41, 45] and to a direct measurement of the coefficient d [37].

Table 2. Contribution to the hyperpolarizability at the magic wavelength from two-photon resonances.

Resonance	Frequency/MHz	Hyperp./µHz
$6s6p\,^3P_0$-$6s8p\,^3P_0$	394 615 049.5(1)	−1.33(6)
$6s6p\,^3P_0$-$6s8p\,^3P_2$	397 484 603.3(3)	0.26(3)
	397 480 706.7(1)	0.094(9)
$6s6p\,^3P_0$-$6s5f\,^3F_2$	391 908 676(4)	−0.06(6)
	391 910 851(10)	0.002(7)

In this measurement the lattice had a frequency of 394 798 267.7 MHz, with less than 1 MHz drift during the whole campaign. Atoms are loaded in the lattice at about $U_0 = 235E_\mathrm{r}$ and afterwards the depth can be either maintained at this level or raised up to $U_0 = 400E_\mathrm{r}$. The lattice is obtained by a titanium-sapphire laser whose spectrum is cleaned by a volume Bragg grating with a bandwidth of 20 GHz. Lattice depth is modulated by acting on an acousto-optic modulator on the lattice laser. The lattice frequency is stabilized on an ultrastable cavity [47] and continuously measured with the optical comb. The trapping conditions U_0, ξ and n are measured by sidebands spectroscopy [48] before and after each run. The typical trapping conditions at low depth are $U_0 = 235(1)E_\mathrm{r}$, $\xi = 0.73(1)$ and $n = 2.1(2)$.

The differential light shift data is corrected for the density shift and then fitted to the model of equation (3) to estimate $a\Delta\nu$. Equation (3) is then used to estimate the shift from the trapping conditions U_0, ξ and n measured for each run. The average lattice shift for the campaign is $7.6(2.0) \times 10^{-17}$, dominated by the quadratic term. Using $a = 27(3)$ mHz GHz^{-1} [27] we can also estimate the magic frequency $\nu_{\mathrm{magic}} = 394\,798\,270(3)$ MHz even if it does not directly impact our light shift determination. This value agrees to the measurements reported by other groups [17, 41, 43] but not with the value of [37].

In our setup the atomic temperature depends on loading conditions and does not vary significantly with lattice depth. The model of [43] requires a linear dependence of the atomic temperature with lattice depth and cannot be used for the data presented here. [37] presents a model of which equation (3) is an approximation and we have estimated a difference of $<3 \times 10^{-18}$ between this model and our analysis.

3.3. Zeeman shift

During spectroscopy we apply a magnetic field of about 25 µT that splits the two π-transitions $^1\mathrm{S}_0(m_F = \pm 1/2)$–$^3\mathrm{P}_0(m_F = \pm 1/2)$ by about 50 Hz from the center. This split is measured for each run with a typical uncertainty of 0.2 Hz. It is used to calculate a quadratic Zeeman shift using the coefficient $a_\mathrm{Z} = -1.531(2)$ µHz/Hz^2 [2]. We have not observed a significant polarization-dependant vector shift from the lattice laser on the magnetic splitting and we assigned a contribution to the Zeeman shift uncertainty of 1×10^{-19} from this effect. The total mean quadratic Zeeman shift is $-6.93(14) \times 10^{-18}$.

3.4. Blackbody radiation shift

The frequency shift due to the environment's blackbody radiation is calculated using the known differential scalar polarizability $\Delta\alpha(0)/h = 36.2612(7) \times 10^{-7}$ Hz V^{-2} m^2 [49] and dynamic correction $\eta(T = 300\ \mathrm{K}) = 0.0180(4)$ [50]. Ten platinum-resistance thermometers measure the vacuum-chamber temperature, including spots near heat sources (e.g. magnetic-field coils) and far away from them. Temperatures are acquired every 80 s, and for each acquisition a frequency shift is calculated where the temperature uncertainty is assigned assuming a rectangular probability distribution between the coldest and hottest readings [27, 51]. We also considered a shift coming from the blackbody radiation emitted from the atomic oven at 700(10) K. The oven temperature is measured with a thermocouple and its uncertainty is dominated by the gradient from the sensor to the nozzle calculated from a simple oven model [52]. Finite-element analysis is used to constrain the effective solid angle of the oven radiation seen by the atoms [53] as in our previous work [27]. The shift from the environment's blackbody radiation is $-235.0(1.2) \times 10^{-17}$ dominated by a typical temperature inhomogeneity of 0.4 K. The shift from the oven is $-1.7(8) \times 10^{-17}$ dominated by the uncertainty on the effective solid angle.

3.5. Static Stark shift

The vacuum-chamber where atoms are trapped is made of aluminum but electric charges may accumulate on the fused-silica windows, causing a static Stark shift. There are two large windows 25 mm from the atoms on the vertical direction, with a bore diameter of 65 mm. In the horizontal direction there are six smaller windows 80 mm from the atoms, with a bore diameter of 40 mm. Two ring electrodes are placed on the large windows and can apply an electric field on the vertical direction. Given this geometry we expect the electric field in the chamber to be predominantly vertical, as possible charges on the horizontal windows are better Faraday-shielded by the chamber metallic structure.

The static Stark shift is thus estimated from a combination of measurements and finite element analysis. The vertical component of the electric field was repeatedly measured during the campaign by applying voltages up to ± 150 V to the ring electrodes [54, 55]. We also accounted that the measured electric field may deviate from the vertical axis up to $\pm$ 30° because of possible patch charges on the large windows. The shift from this electric field observed during the campaign had a maximum absolute value of 3×10^{-17} and a mean of $-0.6(6) \times 10^{-17}$. Its uncertainty is calculated assuming a rectangular probability distribution between the maximum and minimum values of the field observed over several weeks.

We then performed a finite element analysis that constrains the horizontal electric field from possible charges on the small windows resulting in a shift of $-1.0(7) \times 10^{-17}$. We assumed on the horizontal windows a maximum charge density that would cause a shift of 10 kHz if present on the large windows.

The expected shift distribution for both directions is non-Gaussian and we used Monte Carlo methods [56] to assign a combined shift of $-1.6(9) \times 10^{-17}$.

3.6. Background gas shift

The frequency shift due to collisions with background gas is inversely proportional to the mean lifetime in the lattice [2]. The residual background gas in our vacuum chamber is composed by Yb atoms, from the atomic beam, and H_2 molecules, from degassing of stainless-steel fittings, with unknown ratio. We used the coefficient $-1.6(3) \times 10^{-17}$ s, that is deduced from C_6 coefficients [51, 57] theoretically calculated for Yb–Yb collisions [58] and for Yb–H_2 collisions [59]. The C_6 coefficients vary weakly for different background gas species and our calculation is consistent with experiments for Yb–H_2 collisions [2] but its uncertainty includes possible contributions from Yb–Yb collisions. The shift is $-0.5(2) \times 10^{-17}$ from a lifetime in the lattice of $\tau_{\mathrm{lat}} = 3(1)$ s.

3.7. Other shifts

The shift caused by the probe light is $9(5) \times 10^{-19}$ as calculated from the value in [2] applying a scaling inversely proportional to the square of the Rabi time.

The servo error uncertainty is estimated from the average of the error signal during the campaign. A slow control loop is used to cancel the cavity drift making this contribution consistent with zero with an uncertainty of 3×10^{-18}.

All fibre links on the clock laser are actively noise-cancelled and characterized at the 1×10^{-19} level [32].

We calculated line pulling from lattice sidebands and from the π and σ transitions between $m_F = \pm 1/2$ states to be $<2 \times 10^{-19}$, that we take as uncertainty.

The effects of tunnelling and acousto-optic modulator switching were calculated as in [27] to a level of 4×10^{-18}.

3.8. Gravitational redshift

The gravitational redshift with respect to the conventionally adopted equipotential $W_0 = 62\,636\,856.0$ m^2 s^{-2} [35] has been calculated from the gravitational potential difference $C(\mathrm{Yb}) = 2336.28(25)$ m^2 s^{-2}, giving a shift of $2.599\,45(27) \times 10^{-14}$. This measurement was performed as part of the international timescales with optical clocks (ITOC) project with a global navigation satellite system/geoid (GNSS/geoid) approach [60, 61] and it is in agreement with a previous determination [62].

4. Data analysis of the link to the SI second

We measured the ^{171}Yb frequency standard relative to local maser $f(\mathrm{Yb})/f(\mathrm{HM})$ from the modified Julian date, MJD 58 389 to MJD 58 539 (from October 2018 to February 2019). The standard has been operated typically for few hours per

Table 3. Uncertainty budget for the absolute frequency measurement of the ^{171}Yb clock transition via TAI, for each monthly measurement and for the total campaign.

		Oct. 2018	Nov. 2018	Dec. 2018	Jan. 2019	Feb. 2019	Total
	MJD start	58 389	58 419	58 449	58 479	58 514	58 389
	MJD stop	58 419	58 449	58 479	58 514	58 539	58 539
	Yb Uptime	12%	4%	7%	10%	23%	11%
Ratio	Contribution	Uncertainty $\times 10^{17}$					
Yb/HM	Statistical	10	19	15	15	10	6
	Yb syst.	3	3	3	3	2	3
	Comb syst.	8	8	8	8	8	8
HM Extrap.	Drift	2	4	6	4	3	2
	Dead times	23	40	40	30	21	13
HM/UTC(IT)	Steering	1	1	1	1	1	1
UTC(IT)/TAI	Freq. transfer	24	90	70	30	28	14
TAI Extrap.	Drift	—	<1	<1	<1	—	<1
	Dead times	—	52	56	25	—	7
TAI/SI	Statistical	15	13	16	9	11	7
	Systematic	13	12	11	11	12	12
Yb/SI	Total	40	114	100	53	41	26

working day, for a total measurement time of 381 h and a total uptime of 11%.

The ratio $f(\mathrm{Yb})/f(\mathrm{SI})$ has been calculated for each of the five months corresponding to the Circular T number 370 to 374. Table 3 reports the uncertainty budget for each month, as well as for the total campaign.

The analysis follows the measurement model of equation (2) and has been carried out in three steps. In the first step, the ratio $f(\mathrm{Yb})/f(\mathrm{TAI})$ has been calculated over the 5-day grid of Circular T. In the second step, for each 1-month average of $f(\mathrm{TAI})/f(\mathrm{SI})$ in Circular T, we calculated the ratio $f(\mathrm{Yb})/f(\mathrm{SI})$ from the weighted mean of 5-day averages calculated in the first step. Intervals of 5 days without available optical data are ignored and considered dead times. Finally, we took the weighted mean of the monthly calculations to give a result for the total campaign.

The local hydrogen maser, UTC(IT) and TAI are transfer oscillators in the measurement of $f(\mathrm{Yb})/f(\mathrm{SI})$. Their noise is cancelled out in the final calculation and they are not reported in table 3. Dead times in the measurement make this cancellation incomplete and the resulting uncertainty has been assigned to the extrapolation steps.

4.1. Linearization

When analyzing the data we linearize the model equation (2) by moving from each ratio r to the fractional correction $y = r/r_0 - 1$, where r_0 is an arbitrary reference ratio. The total fractional correction $y(f(\mathrm{Yb})/f(\mathrm{SI}))$ can be calculated as the sum of the fractional corrections of each ratio. We choose the reference ratios involving ^{171}Yb to be consistent with the numerical value of the recommended frequency for ^{171}Yb as a secondary representation of the second, $f(\mathrm{Yb}, \mathrm{CIPM2017}) = 518\,295\,836\,590\,863.6(3)$ Hz [63]. The absolute values of all fractional corrections in our analysis are less than 1×10^{-12}, justifying the linear approximation.

4.2. Uncertainty of $f(\mathrm{Yb})/f(\mathrm{HM})$

The ratio $f(\mathrm{Yb})/f(\mathrm{HM})$ is affected by the statistical noise and the systematic uncertainty of the ^{171}Yb standard and of the comb. The combined statistical uncertainty of ^{171}Yb standard and comb has been conservatively estimated as the white frequency component of the observed noise for each run. We expect a contribution of $2 \times 10^{-14}(\tau/\mathrm{s})^{-1/2}$, where τ is the measurement time, from the frequency multiplication of the hydrogen maser at 10 MHz to 250 MHz (repetition rate of the comb). The statistical contribution from the ^{171}Yb optical standard is at the level of $2 \times 10^{-15}/(\tau/\mathrm{s})^{-1/2}$ (compare figure 2). The comb systematic uncertainty in the transfer from the microwave domain to the optical domain has been assessed as 8×10^{-17} by comparison with a second comb. (The use of the comb for optical to optical transfer is better characterized to 3×10^{-19} [31].) The ^{171}Yb systematic uncertainty has been calculated for each run as explained in the previous section.

4.3. Extrapolation over the hydrogen maser

The extrapolation $f(\mathrm{HM}, \mathcal{T}_1)/(\mathrm{HM}, \mathcal{T}_2)$ has been calculated separately for each 5-day interval. Its evaluation includes a deterministic correction for the maser drift and the statistical uncertainty from dead times.

The drift correction can be calculated as $D \times (\langle \mathcal{T}_1 \rangle - \langle \mathcal{T}_2 \rangle)$, where D is the maser drift and $\langle \mathcal{T}_1 \rangle, \langle \mathcal{T}_2 \rangle$ are the barycenters of the two averaging periods $\mathcal{T}_1, \mathcal{T}_2$. Here the maser frequency drift is determined from $f(\mathrm{HM})/f(\mathrm{TAI})$ data calculated from data in the Circular T. For each extrapolation, the drift is measured from a linear fit over a period of 25 d. The typical maser drift for the campaign was 3.5×10^{-16} d^{-1}.

The uncertainty from dead times has been calculated by simulating the maser noise, as presented in [11, 15, 25]. We used the software Stable32 [64] to generate 10^7 points

simulating the maser phase noise with a sample time of 100 s. The instability of the stochastic maser noise is modelled as the quadrature sum of components due to white phase noise $1.5 \times 10^{-13}(\tau/\mathrm{s})^{-1}$, white frequency noise $3.5 \times 10^{-14}(\tau/\mathrm{s})^{-1/2}$, flicker frequency noise 6×10^{-16}, random walk frequency noise $1 \times 10^{-18}(\tau/\mathrm{s})^{1/2}$. This model is based on the characterization of the maser and it is consistent with the observed $f(\mathrm{Yb})/f(\mathrm{HM})$ instability. The generated noise is sampled to simulate $\sim 1 \times 10^4$ repeated averages over the periods $\mathcal{T}_1$, $\mathcal{T}_2$. The uncertainty from dead times is calculated as the sample standard deviation of the difference between the simulated repeated averages.

4.4. Uncertainty of $f(\mathrm{HM})/f(\mathrm{UTC(IT)})$

The steering $f(\mathrm{HM})/f(\mathrm{UTC(IT)})$ was calculated continuously from the correction applied by the auxiliary output generator that has an instability of $3 \times 10^{-13}(\tau/\mathrm{s})^{-1}$ (uncertainty $<1 \times 10^{-18}$ for averages over 5 d) and a systematic uncertainty of 1×10^{-17}.

4.5. Uncertainty of $f(\mathrm{UTC(IT)})/f(\mathrm{TAI})$

The frequency ratio $f(\mathrm{UTC(IT)})/f(\mathrm{TAI})$ was calculated for 5-day intervals corresponding to the data in Circular T. The recommended formula for calculating the uncertainty in the satellite frequency transfer is [65]:

$$u_{\mathrm{UTC(IT)/TAI}}(\tau) = \frac{\sqrt{2}u_{\mathrm{A}}}{\tau_0} \times \left(\frac{\tau}{\tau_0}\right)^{-0.9}, \qquad (4)$$

where $u_{\mathrm{A}} = 0.4$ ns is the type A uncertainty of the time transfer from UTC(IT) to TAI as reported in Circular T, $\tau_0 = 5$ d and τ is the total measurement time. Type B uncertainties for the time transfer reported in Circular T represent a calibration offset in time and do not affect the frequency measurement.

4.6. Extrapolation over TAI

The extrapolation $f(\mathrm{TAI}, \mathcal{T}_2)/f(\mathrm{TAI}, \mathcal{T}_3)$ has been calculated for each month. This step was unnecessary for the months October 2018 and February 2019 which have data for all 5-day intervals.

TAI inherits the instability of the free atomic timescale (Echelle Atomique Libre, EAL). The EAL instability model is reported in the Circular T explanatory supplement as the quadrature sum of white frequency noise $1.7 \times 10^{-15}(\tau/\mathrm{d})^{-1/2}$, flicker frequency noise 3.5×10^{-16}, random-walk frequency noise $2 \times 10^{-17}(\tau/\mathrm{d})^{1/2}$. The uncertainty from dead times has been calculated from this noise similarly to the extrapolation over the local hydrogen maser, with 10 000 phase points simulated in steps of 1 d. The drift contribution is calculated from $f(\mathrm{TAI})/f(\mathrm{SI})$ and it is negligible for this campaign.

4.7. Uncertainty of $f(\mathrm{TAI})/f(\mathrm{SI})$

The frequency deviation of TAI relative to the SI second is reported directly in Circular T for each month. The BIPM calculates it from the contribution of primary and secondary frequency standards up to one year before the reporting period. The primary frequency standards reporting data during this campaign were the Cs Fountains PTB-CSF1, PTB-CSF2 [66], SYRTE-FO1, SYRTE-FO2, SYRTE-FOM [67], SU-CsFO2 [68], NIM5 [69] and the Cs thermal beams PTB-CS1 and PTB-CS2 [70]. The Cs Fountain ITCsF2 [28] did not contributed during the campaign but submitted data within the previous year. The Rb fountain SYRTE-FORb [71] contributed as a secondary frequency standard. Moreover, the ^{87}Sr optical lattice frequency standards NICT-Sr1 [11, 16, 23] and SYRTE-SrB [24] contributed as secondary frequency standards. SYRTE-SrB contributed to the Circular T 372 (December 2018). NICT-Sr1 contributed to the Circular T 372, 373 and 374 (December 2018, January 2019 and February 2019) as well as submitting data within the previous year in Circular T 371.

The Circular T reports only the total uncertainty of the ratio $f(\mathrm{TAI})/f(\mathrm{SI})$. We estimated the systematic uncertainty for this ratio from the type B uncertainty of the standards reported in each Circular T and their weight [13, 19]. This calculation included the uncertainties of the secondary representations of the second and assumed the frequency shift for each standard uncorrelated (this is an adequate approximation for the uncertainties affecting Cs fountains). We then chose the statistical uncertainty to recover the total uncertainty as calculated by the BIPM.

4.8. Correlations and averaging

In our analysis we considered correlations between available data, as they are important in the uncertainty analysis. Weighted averages were calculated using the Gauss–Markov theorem, or generalized least-square fit [72, 73]. This algorithm is the same suggested for the least-square analysis of frequency standards [7].

We assumed the systematic uncertainties in each ratio to be correlated in time. In this sense they do not average down. This approximation is also used for the systematic uncertainty we estimated for the $f(\mathrm{TAI})/f(\mathrm{SI})$ ratio.

The measurements of the maser drift for each 5-day interval are correlated between each other because they derive from the same data set. The resulting correlations in the maser extrapolations vary depending on the barycenter of each datum.

We consider dead-time uncertainties calculated for different periods of time uncorrelated because they represent statistical noise and we average data without overlaps.

The ratio $f(\mathrm{UTC(IT)})/f(\mathrm{TAI})$ is calculated from the time-difference (phase) data of the satellite link. The conversion from phase to frequency brings negative correlation in the frequency data (consecutive frequency points share the middle phase point). We took this effect into account by numerically calculating the correlations of $f(\mathrm{UTC(IT)})/f(\mathrm{TAI})$ 5-day averages that replicate equation (4) when used with the law of propagation of uncertainty. We note that equation (4) is valid only for averaging with uniform weights. Introducing correlations allows us to extend equation (4) to the case of non-uniform weights while keeping consistency with the

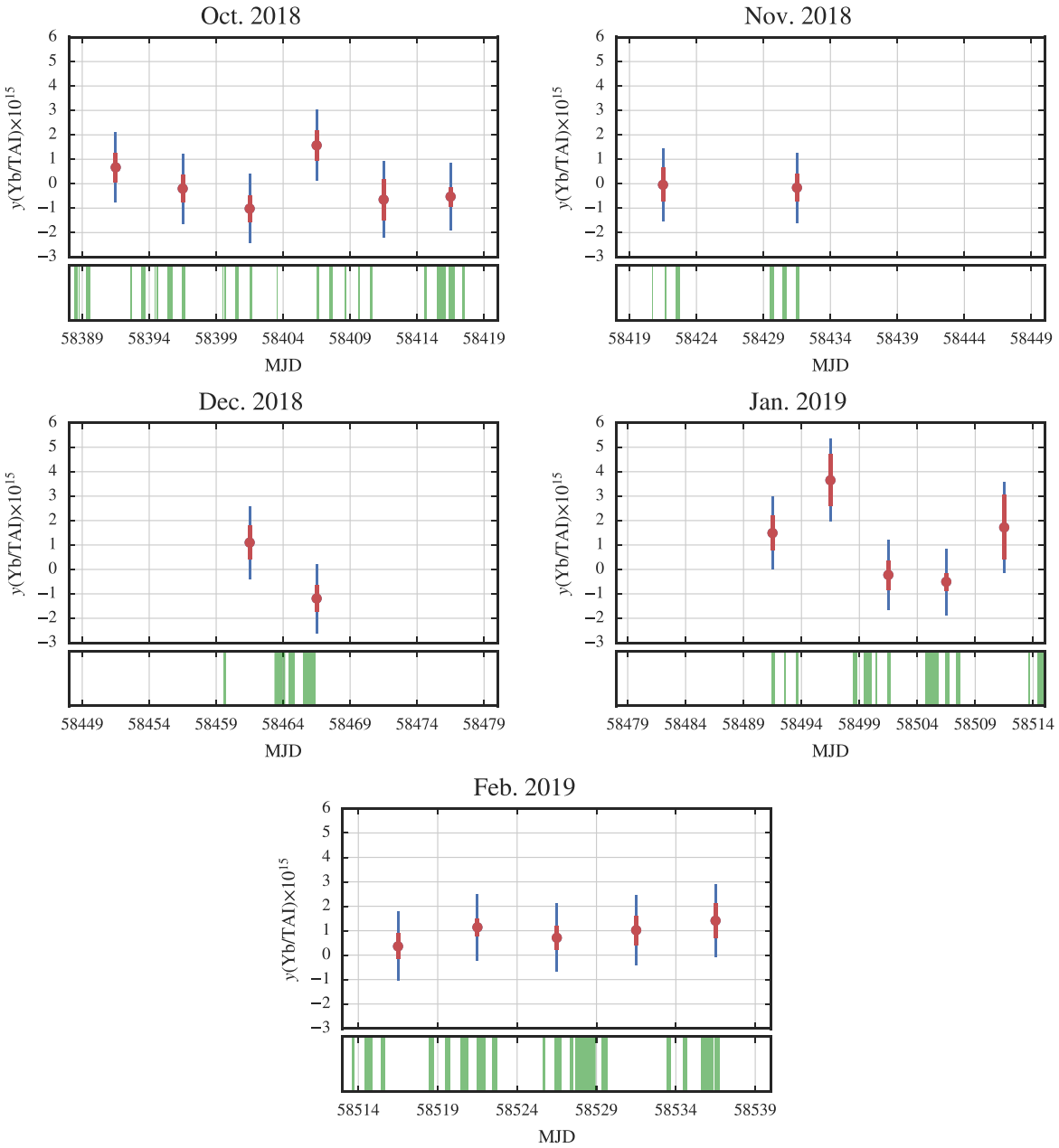

Figure 3. Fractional corrections $y(f(\mathrm{Yb})/f(\mathrm{TAI}))$ averaged every 5 days for each month of the campaign. Green shaded regions at the bottom of each plot represent the uptime of the ^{171}Yb frequency standard. Blue bars represent the total combined uncertainty for each average. Red thick bars denote the uncertainty of all components excluding the satellite frequency transfer to TAI.

recommended formula. This allows us to calculate weighted means, with a lower combined uncertainty for the final result.

The correlations observed between 5-day averages of $f(\mathrm{Yb})/f(\mathrm{TAI})$ range between -37% and 5.8%. The correlations observed between 1-month averages of $f(\mathrm{Yb})/f(\mathrm{SI})$ range between -5.9% and 13.4%.

5. Results and discussion

The fractional corrections $y(f(\mathrm{Yb})/f(\mathrm{TAI}))$ averaged every 5 days are shown in figure 3. The shaded regions in the figures represent the intervals where the measurements of the ratio $f(\mathrm{Yb})/f(\mathrm{HM})$ were available, as limited by the uptime of the ^{171}Yb frequency standard.

The fractional corrections $y(f(\mathrm{Yb})/f(\mathrm{SI}))$ averaged for each month of the campaign are shown in figure 4. The weighted average of the 5 monthly measurements is $y(f(\mathrm{Yb})/f(\mathrm{SI})) = 2(26) \times 10^{-17}$ and is shown as the shaded region in the figure. The Birge ratio for the fit is $\sqrt{\chi^2/n} = 1.011$ with $n = 4$ degrees of freedom. The absolute frequency measurement result is $f(\mathrm{Yb}) = 518\,295\,836\,590\,863.61(13)$ Hz, with a relative combined standard uncertainty of 2.6×10^{-16}.

Operating the ^{171}Yb optical lattice frequency standard for five months made it possible to average the noise of

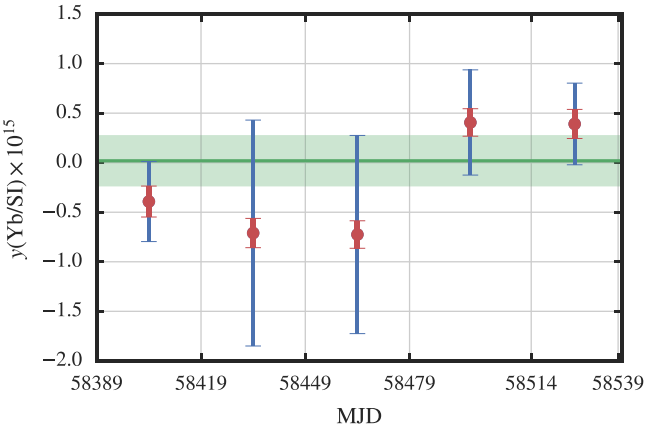

Figure 4. Fractional corrections $y(f(\mathrm{Yb})/f(\mathrm{SI}))$ averaged every month of the campaign. Blue bars denote the total combined uncertainty, while red thick bars denote only the systematic contributions. The green shaded region denotes the weighted average for the campaign with its uncertainty.

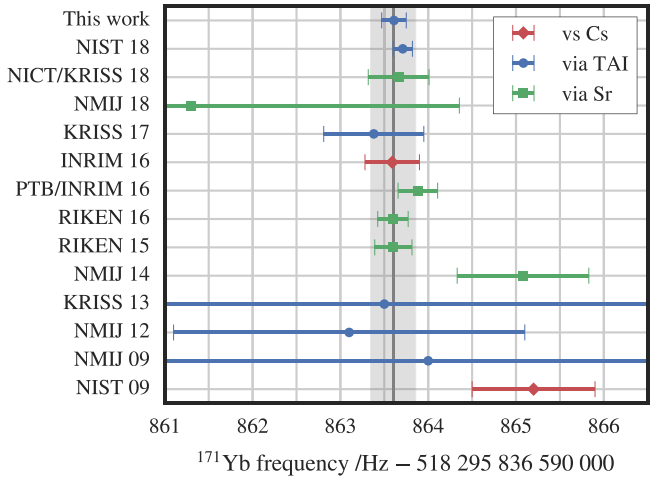

Figure 5. Absolute frequency of the $^1S_0$–$^3P_0$ transition of ^{171}Yb as measured by NIST [19, 74], the National Metrology Institute of Japan (NMIJ) [9, 75], the Korea Research Institute of Standards and Science (KRISS) [10, 17], INRIM [27] and this work. Also reported are absolute frequencies deduced from optical ratios with ^{87}Sr frequency standards as measured by NMIJ [76, 78], RIKEN [41, 77], PTB and INRIM [29], NICT and KRISS [79]. The gray shaded region denotes the recommended frequency for ^{171}Yb as a secondary representation of the second with its uncertainty 5×10^{-16}.

the satellite frequency transfer to TAI to an uncertainty of 1.4×10^{-16} that is the largest contribution to the uncertainty budget. Furthermore, with an uptime of the ^{171}Yb standard of 11%, the extrapolation using the hydrogen maser as a flywheel contributes a similar uncertainty of 1.3×10^{-16}. The link to TAI allows us to trace the measurement to all the primary and secondary standards contributing to the Circular T, where the Cs fountains at LNE-SYRTE and PTB carry the largest weight. We estimated the systematic uncertainties of these standards to contribute an uncertainty of 1.2×10^{-16} that is the state-of-the-art for the realization of the SI unit of frequency.

We have calculated negligible correlations (<0.5%) between the measurement presented in this work and previous measurements involving the same ^{171}Yb frequency standard [27, 29]. Correlations with other measurements using links to TAI and data in Circular T have not yet been estimated. For example, the correlation with the measurement in [19] could be as high as 29% if we assume the systematic uncertainty of the primary and secondary frequency standards contributing to TAI for the two measurements totally correlated. These correlations need to be properly accounted for to not underestimate the uncertainty of the recommended values of the secondary representations of the second from least-square analysis [7].

Our result is in good agreement with the recommended frequency for ^{171}Yb as a secondary representation of the second and previous measurements. Figure 5 shows a comparison with measurements relative to Cs fountains [27, 74], carried out via TAI [9, 10, 17, 19, 75] or deduced from optical ratios with ^{87}Sr frequency standards [29, 41, 76–79]. The recommended frequency of ^{87}Sr as a secondary representation of the second $f(\mathrm{Sr, CIPM2017}) = 429\,228\,004\,229\,873.00(17)$ Hz, with its uncertainty [63], has been used to convert optical frequency ratios. The grey shaded region in the figure shows the recommended frequency for ^{171}Yb as a secondary representation of the second.

In the analysis described in section 4, the extrapolation over the local hydrogen maser was carried out only for periods of 5 days. In an alternative analysis, we extrapolated the local hydrogen maser directly to one month, avoiding the need to extrapolate over TAI. From this simpler analysis we obtained $y(f(\mathrm{Yb})/f(\mathrm{SI})) = -12(27) \times 10^{-17}$, a result in agreement and with similar uncertainty relatively to the main analysis. However, we believe the analysis extrapolating with both the local maser and TAI is more reliable as it does not depend on the performance of a single maser over long periods of time.

As ^{87}Sr optical lattice frequency standards NICT-Sr1 and SYRTE-SrB contributed to TAI we can alternatively perform a direct calculation of the $f(\mathrm{Yb})/f(\mathrm{Sr})$ ratio instead of the absolute frequency $f(\mathrm{Yb})/f(\mathrm{SI})$. We calculated a fractional correction $y(f(\mathrm{Yb})/f(\mathrm{Sr})) = -46(43) \times 10^{-17}$ averaged over December 2018, January 2019, and February 2019 that corresponds to an optical ratio $f(\mathrm{Yb})/f(\mathrm{Sr}) = 1.207\,507\,039\,343\,337\,19(52)$, in agreement with previous measurements [29, 41, 76–79]. This ratio measurement is unaffected by the uncertainty in the ^{87}Sr secondary representation of the second, even if it is included in the ^{87}Sr optical lattice frequency standards contribution to TAI. The fractional uncertainty of the ratio is dominated by the satellite frequency link as the averaging time is shorter than the full campaign.

6. Conclusions

We have reported an absolute frequency measurement of the unperturbed optical clock transition $^1S_0$–$^3P_0$ in ^{171}Yb performed with an optical lattice frequency standard and a link to TAI over 5 months. The long campaign duration highlighted the importance of properly accounting for the uncertainty introduced by the intermittent operation of the optical standard and to properly account for the correlations in the data.

Moreover, we showed that from the same link it is possible to calculate optical frequency ratios, since Circular T included data from optical frequency standards.

The absolute frequency measurement has a fractional standard uncertainty of 2.6×10^{-16} that is similar to that of absolute frequency measurements relative to local Cs fountains [24, 26] and to that of recent measurements carried out with a link to TAI [15, 16, 19]. For this campaign we have evaluated the systematic corrections of the ^{171}Yb optical lattice frequency standard that contribute to the absolute frequency measurement with a fractional uncertainty of 2.8×10^{-17}.

Our new absolute frequency measurement further supports the consistency of optical frequency standards and strengthens the case for a redefinition of the SI second based on an optical transition [5]. It is expected that it will contribute to the updates of the list of recommended values of standard frequencies [6]. Moreover, our work has been an important step for submitting the ^{171}Yb standard data to the BIPM and for contributing to international timescales as a secondary representation of the second.

Acknowledgments

We thank Elio Bertacco, Alberto Mura and Marco Sellone for help and Cecilia Clivati for helpful discussions and careful reading of the manuscript. We also thank the groups operating primary and secondary frequency standards in national metrology institutes around the world; our measurement would have been impossible without the availability of their data in the Circular T.

We acknowledge funding from the European Metrology Program for Innovation and Research (EMPIR) project 15SIB03 OC18, from the Horizon 2020 Marie Sklodowska–Curie Research and Innovation Staff Exchange (MSCA-RISE) project Q-SENSE (Grant Agreement No. 691156), from the Italian Space Agency (ASI) funding DTF-Matera, from the EMPIR project 18SIB05 ROCIT. The EMPIR initiative is co-funded by the European Union's Horizon 2020 research and innovation programme and the EMPIR Participating States.

The datasets for the absolute frequency measurement in this works are openly available [80].

ORCID iDs

Marco Pizzocaro https://orcid.org/0000-0003-2353-362X

References

[1] Wynands R and Weyers S 2005 *Metrologia* **42** S64
[2] McGrew W F *et al* 2018 *Nature* **564** 87–90
[3] Huntemann N, Sanner C, Lipphardt B, Tamm C and Peik E 2016 *Phys. Rev. Lett.* **116** 063001
[4] Ushijima I, Takamoto M, Das M, Ohkubo T and Katori H 2015 *Nat. Photon.* **9** 185–9
[5] Riehle F, Gill P, Arias F and Robertsson L 2018 *Metrologia* **55** 188
[6] Consultative Committee for Time and Frequency (CCTF) 2017 *Report of the 21st Meeting (8–9 June 2017) to the International Committee for Weights and Measures* (available from: www.bipm.org)
[7] Margolis H S and Gill P 2015 *Metrologia* **52** 628
[8] Hong F L, Inaba H, Hosaka K, Yasuda M and Onae A 2009 *Opt. Express* **17** 1652–9
[9] Yasuda M *et al* 2012 *Appl. Phys. Express* **5** 102401
[10] Park C Y *et al* 2013 *Metrologia* **50** 119
[11] Hachisu H and Ido T 2015 *Japan. J. Appl. Phys.* **54** 112401
[12] Huang Y, Guan H, Liu P, Bian W, Ma L, Liang K, Li T and Gao K 2016 *Phys. Rev. Lett.* **116** 013001
[13] Hachisu H, Petit G and Ido T 2016 *Appl. Phys.* B **123** 34
[14] Dubé P, Bernard J E and Gertsvolf M 2017 *Metrologia* **54** 290–8
[15] Baynham C F A *et al* 2017 *J. Mod. Opt.* **65** 585–91
[16] Hachisu H, Petit G, Nakagawa F, Hanado Y and Ido T 2017 *Opt. Express* **25** 8511–23
[17] Kim H, Heo M S, Lee W K, Park C Y, Hong H G, Hwang S W and Yu D H 2017 *Japan. J. Appl. Phys.* **56** 050302
[18] Petit G and Panfilo G 2018 Optimal traceability to the SI second through TAI *2018 European Frequency and Time Forum* pp 185–7
[19] McGrew W F *et al* 2019 *Optica* **6** 448–54
[20] Arias E F, Panfilo G and Petit G 2011 *Metrologia* **48** S145–53
[21] BIPM Circular T (available from: www.bipm.org)
[22] Bilicki S, Bookjans E, Vallet G, Abgrall M, Targat R L and Lodewyck J 2017 Contributing to TAI with Sr optical lattice clocks *2017 Joint Conf. of the European Frequency and Time Forum and IEEE Int. Frequency Control Symp.* pp 815–6
[23] Hachisu H, Nakagawa F, Hanado Y and Ido T 2018 *Sci. Rep.* **8** 4243
[24] Lodewyck J *et al* 2016 *Metrologia* **53** 1123
[25] Yu D H, Weiss M and Parker T E 2007 *Metrologia* **44** 91
[26] Grebing C, Al-Masoudi A, Dörscher S, Häfner S, Gerginov V, Weyers S, Lipphardt B, Riehle F, Sterr U and Lisdat C 2016 *Optica* **3** 563–9
[27] Pizzocaro M, Thoumany P, Rauf B, Bregolin F, Milani G, Clivati C, Costanzo G A, Levi F and Calonico D 2017 *Metrologia* **54** 102
[28] Levi F, Calonico D, Calosso C E, Godone A, Micalizio S and Costanzo G A 2014 *Metrologia* **51** 270
[29] Grotti J *et al* 2018 *Nat. Phys.* **14** 437–41
[30] Pizzocaro M, Costanzo G A, Godone A, Levi F, Mura A, Zoppi M and Calonico D 2012 *IEEE Trans. Ultrason. Ferroelectr. Freq. Control* **59** 426–31
[31] Barbieri P, Clivati C, Pizzocaro M, Levi F and Calonico D 2019 *Metrologia* **56** 045008
[32] Rauf B, López M C V, Thoumany P, Pizzocaro M and Calonico D 2018 *Rev. Sci. Instrum.* **89** 033103
[33] Bauch A *et al* 2005 *Metrologia* **43** 109–20
[34] Lewandowski W, Matsakis D, Panfilo G and Tavella P 2008 *IEEE Trans. Ultrason. Ferroelectr. Freq. Control* **55** 750–60
[35] General Conference on Weights and Measures (CGPM) 2018 *Resolution 2 of its 26th Meeting* (available from: www.bipm.org)
[36] Yanagimoto R, Nemitz N, Bregolin F and Katori H 2018 *Phys. Rev.* A **98** 012704
[37] Nemitz N, Jørgensen A A, Yanagimoto R, Bregolin F and Katori H 2019 *Phys. Rev.* A **99** 033424
[38] Lemke N D, von Stecher J, Sherman J A, Rey A M, Oates C W and Ludlow A D 2011 *Phys. Rev. Lett.* **107** 103902
[39] Lee S, Park C Y, Lee W K and Yu D H 2016 *New J. Phys.* **18** 033030

[40] Bregolin F 2019 ^{171}Yb optical frequency standards towards the redefinition of the second *PhD Thesis* Politecnico di Torino
[41] Nemitz N, Ohkubo T, Takamoto M, Ushijima I, Das M, Ohmae N and Katori H 2016 *Nat. Photon.* **10** 258–61
[42] Katori H, Ovsiannikov V D, Marmo S I and Palchikov V G 2015 *Phys. Rev.* A **91** 052503
[43] Brown R C *et al* 2017 *Phys. Rev. Lett.* **119** 253001
[44] Barber Z W *et al* 2008 *Phys. Rev. Lett.* **100** 103002
[45] Kobayashi T, Akamatsu D, Hisai Y, Tanabe T, Inaba H, Suzuyama T, Hong F, Hosaka K and Yasuda M 2018 *IEEE Trans. Ultrason. Ferroelectr. Freq. Control* **65** 2449–58
[46] McDonald M, McGuyer B H, Iwata G Z and Zelevinsky T 2015 *Phys. Rev. Lett.* **114** 023001
[47] Milani G, Rauf B, Barbieri P, Bregolin F, Pizzocaro M, Thoumany P, Levi F and Calonico D 2017 *Opt. Lett.* **42** 1970–3
[48] Blatt S, Thomsen J W, Campbell G K, Ludlow A D, Swallows M D, Martin M J, Boyd M M and Ye J 2009 *Phys. Rev.* A **80** 052703
[49] Sherman J A, Lemke N D, Hinkley N, Pizzocaro M, Fox R W, Ludlow A D and Oates C W 2012 *Phys. Rev. Lett.* **108** 153002
[50] Beloy K, Hinkley N, Phillips N B, Sherman J A, Schioppo M, Lehman J, Feldman A, Hanssen L M, Oates C W and Ludlow A D 2014 *Phys. Rev. Lett.* **113** 260801
[51] Falke S *et al* 2014 *New J. Phys.* **16** 073023
[52] Schioppo M, Poli N, Prevedelli M, Falke S, Lisdat C, Sterr U and Tino G M 2012 *Rev. Sci. Instrum.* **83** 103101
[53] Abdel-Hafiz M *et al* 2019 (arXiv:1906.11495)
[54] Lodewyck J, Zawada M, Lorini L, Gurov M and Lemonde P 2012 *IEEE Trans. Ultrason. Ferroelectr. Freq. Control* **59** 411–5
[55] Beloy K, Zhang X, McGrew W F, Hinkley N, Yoon T H, Nicolodi D, Fasano R J, Schäffer S A, Brown R C and Ludlow A D 2018 *Phys. Rev. Lett.* **120** 183201
[56] BIPM, IEC, IFCC, ILAC, ISO, IUPAC, IUPAP and OIML 2008 Evaluation of measurement data–supplement 1 to the 'guide to the expression of uncertainty in measurement'–propagation of distributions using a Monte Carlo method Joint Committee for Guides in Metrology *JCGM 101* (available from: www.bipm.org)
[57] Gibble K 2013 *Phys. Rev. Lett.* **110** 180802
[58] Porsev S G, Safronova M S, Derevianko A and Clark C W 2014 *Phys. Rev.* A **89** 012711
[59] Milani G 2018 Realization of advanced 171Yb optical lattice frequency standard *PhD Thesis* Politecnico di Torino
[60] Margolis H *et al* 2013 International timescales with optical clocks (ITOC) *European Frequency and Time Forum Int. Frequency Control Symp., 2013 Joint* pp 908–11
[61] Denker H, Timmen L, Voigt C, Weyers S, Peik E, Margolis H S, Delva P, Wolf P and Petit G 2018 *J. Geod.* **92** 487–516
[62] Calonico D, Cina A, Bendea I H, Levi F, Lorini L and Godone A 2007 *Metrologia* **44** L44
[63] BIPM 2018 *Recommended values of standard frequencies* (available from: www.bipm.org)
[64] IEEE UFFC-S 2019 *Stable32–Software for Frequency Stability Analysis* (available from: ieee-uffc.org)
[65] Panfilo G and Parker T E 2010 *Metrologia* **47** 552–60
[66] Weyers S, Gerginov V, Kazda M, Rahm J, Lipphardt B, Dobrev G and Gibble K 2018 *Metrologia* **55** 789–805
[67] Guena J *et al* 2012 *IEEE Trans. Ultrason. Ferroelectr. Freq. Control* **59** 391–409
[68] Blinov I Y, Boiko A I, Domnin Y S, Kostromin V P, Kupalova O V and Kupalov D S 2017 *Meas. Tech.* **60** 30–6
[69] Fang F, Li M, Lin P, Chen W, Liu N, Lin Y, Wang P, Liu K, Suo R and Li T 2015 *Metrologia* **52** 454–68
[70] Bauch A 2005 *Metrologia* **42** S43–54
[71] Guéna J, Abgrall M, Clairon A and Bize S 2014 *Metrologia* **51** 108
[72] Luenberger D G 1998 *Optimization by Vector Space Methods* (New York: Wiley)
[73] Cox M G, Eiø C, Mana G and Pennecchi F 2006 *Metrologia* **43** S268
[74] Lemke N D, Ludlow A D, Barber Z W, Fortier T M, Diddams S A, Jiang Y, Jefferts S R, Heavner T P, Parker T E and Oates C W 2009 *Phys. Rev. Lett.* **103** 063001
[75] Kohno T, Yasuda M, Hosaka K, Inaba H, Nakajima Y and Hong F L 2009 *Appl. Phys. Express* **2** 072501
[76] Akamatsu D, Yasuda M, Inaba H, Hosaka K, Tanabe T, Onae A and Hong F L 2014 *Opt. Express* **22** 32199
[77] Takamoto M *et al* 2015 *C. R. Phys.* **16** 489–98
[78] Akamatsu D, Kobayashi T, Hisai Y, Tanabe T, Hosaka K, Yasuda M and Hong F 2018 *IEEE Trans. Ultrason. Ferroelectr. Freq. Control* **65** 1069–75
[79] Fujieda M *et al* 2018 *IEEE Trans. Ultrason. Ferroelectr. Freq. Control* **65** 973–8
[80] Pizzocaro M, Bregolin F, Barbieri P, Rauf B, Levi F and Calonico D 2019 (https://doi.org/10.5281/zenodo.3453859)